# Health Monitoring of Joints Using Dynamic End Effects

Baruch Karp, Daniel Rittel, David Durban

B. Karp, D. Durban: *Faculty of Aerospace Engineering, Technion – Israel Institute of Technology, Haifa 32000, Israel.*

D. Rittel: *Faculty of Mechanical Engineering, Technion – Israel Institute of Technology, Haifa 32000, Israel.*

Corresponding Author: B. Karp, *E-mail: baruch@tx.technion.ac.il*

**Abstract**

An experimental feasibility study for monitoring integrity of structural joints, based on measurement of end effects, is reported. The methodology is based on end effects excited when edge conditions deviate from baseline boundary data. It was found that by attaching standard strain gauges to a beam at the immediate vicinity of the joint, it is possible to identify small changes in the clamping condition, either by static loading or by dynamic excitation of the structure. End effects measured on the surface are viewed as the joint health signature. High sensitivity of surface strains to small changes in end conditions can be utilized in structural health monitoring systems to identify low levels of damage for structural joints (realized either by screws, welding, riveting, or bonding).

## 1. Introduction

Condition-based real-time maintenance of structural components is a relatively new arena enabling cost-effective maintenance and improved functional reliability of the structure. Emergence of this field has been enabled by intensive developments of structural health monitoring (SHM) systems during the last few decades. Several recent reviews discuss methods employed in detection, allocation, and evaluation of various types of structural damage ([1]-[6]). Basically, SHM systems consist of a physical device for data collection and a signal processing computer along with an appropriate algorithm. Efficient identification of the onset of damage, or deterioration, at the earliest possible stage,

centers on the sensitivity of a selected diagnostic parameter of structural response to the type of damage to be detected. That sensitivity is reflected in the design of the monitoring device and in the selected signal processing algorithm.

Currently, SHM systems rely mainly on three diagnostic parameters considered as structural markers: modal properties of vibrating structures, propagation of Lamb waves, and impedance of the structure as sensed by attached PZT wafers. Recently, Pandurangan and Buckner [7] suggested the use of modal damping ratios as another marker for monitoring single-lap adhesive joints. Their experiments reveal that the sensitivity of this method is favorable in comparison with frequency-based methods.

In the present paper we report on a feasibility study for employing *end effects* as an alternative diagnostic parameter (structural marker) for health monitoring of structural joints. In a sense, these end effects can be considered as a special case of Lamb waves spectra. Nevertheless, to the authors' best knowledge, *propagating waves* are dominant in the design and analysis of existing SHM methods (e.g., [6]) whereas the emphasis here is on end effects associated with *evanescent waves* (e.g., [8]).

The proposed methodology is based on the known observation of high sensitivity of the *near field* to details of end data. Evanescent waves are generated at the ends of waveguides due to spatial incompatibility between the end data and the propagating modes. In statics this pattern falls under the study of Saint-Venant's principle. In dynamics, although no agreed upon analogy to the static Saint-Venant principle has yet been found [9], that sensitivity has been observed in problems related to waveguides as, for example, in the split Hopkinson bar instrumentation. Traditionally, both in statics and in dynamics of structures, reliance on the response of the structure within the near field has not been of practical interest. Here, it is indeed this sensitivity to end data that is taken advantage of. End effects are regarded as the *joint signature* and contain key data

pertaining to the integrity of edge fixation. To investigate in laboratory tests the effect of damaged end conditions on near field effects, a cantilever beam with controlled damage of the clamping conditions was chosen.

The dynamic response of a cantilever beam has been experimentally examined to demonstrate near field sensitivity to details of the end conditions (Fig. 1). “End conditions” are perceived here as a manifestation of the details of the joint, with possible deviations from the designed original configuration. In view of the analytical similarity between static and dynamic end effects (exponential decay in the axial direction), both static and dynamic experiments were performed. In the static experiments a weight was attached to the free end of the beam. In the dynamic experiments a short rod was dropped to hit the same free end of the beam. Strains along the centerline of the beam were measured for repeated identical excitations with (controlled) different clamping conditions of the built-in end. Five strain gauges were attached to the upper surface of the beam, three located within the immediate vicinity of the clamped end (near field) and two at a distance from it (far field).

Clamping of the beam is achieved by six screws, shown in Fig. 1. Various combinations of tightness of the screws were considered as simulating different clamping conditions. It is noted here that "clamping" is a term used in practice with no definite meaning within the theory of elasticity. For the purpose of the present work the phrase *clamping condition* will be used to discriminate between various ways in which end fixation is realized, all of which could be considered as "clamping" for practical engineering purposes. Various levels of tightness of the screws can be regarded as different end conditions and as artificially induced damage to the joint, simulating events such as loosening of bolts, debonding, cracking, or loss of rivets. Recalling the axial decay of eigenfunctions in static fields, and the existence of evanescent waves in the

dynamic response, it is expected that at least part of the strain history readings will reflect the controlled changes in clamping conditions.

The main result emerging from this study is that simple experimental techniques, along with monitoring of surface strains in the near field, enable the identification of even minor changes in the joint condition. In the static experiments the condition of completely and partially loose screws was identified. In the dynamic experiments completely loose screws were identified clearly with less conclusive results for partially loose screws. These observations agree well with the analysis of end effects given in the first part of the paper. In both the static and dynamic experiments, the far field measured data of strains was found to be insensitive to fine details in the clamping condition. Far field response is influenced only when more than one screw is missing. This condition departs considerably from what would be considered as clamping from the engineering practice point of view.

## 2. Analytical construction of end effects

End effect is a common synonym to Saint-Venant's principle (SVP), according to which the strains and the stresses at points located far from the loaded end are determined uniquely by statical equivalents of the applied edge load and are not affected by the spatial distribution of the load. End effects can be viewed as the near edge strain perturbations, induced by small changes in end data, and decaying in the axial direction. Here, the formal representation of these end effects is summarized briefly, both for static and dynamic loadings.

### *2.1. Static End Effects*

The solution of plate problems is commonly partitioned into two parts (e.g., [10]) the *inner* solution and the *outer* solution. The simplest inner solutions of plane problems are

given analytically by polynomial solutions of the bi-harmonic equation. The axial strain for an elastic, isotropic cantilever plate subjected to bending by a dead load $P$ applied at its free end, under plane strain conditions, is given by

$$\varepsilon_x(x,y) = \frac{(1-\nu^2)(l-x)P}{EI} y \tag{1}$$

where $E$ is Young's modulus, $\nu$ is Poisson's ratio, $I$, and $l$ are the inertia, and length of the beam, respectively. Here $x,y$ denote the axial and transverse coordinates with the origin at the center of the built-in end (see Fig. 1). Expression (1) is exact everywhere within the plate as long as the boundary conditions comply with this solution – linearly distributed axial stress and parabolic distribution of shear stress at the clamped end, and zero axial stress with a parabolic distribution of the shear stress at the loaded end.

If clamping is realized in a way that the distribution of the boundary stresses across the thickness deviates from the inner solution, end effects will be generated and expression (1) will no longer be accurate close to the vicinity of the edge. The actual stress at the end can be viewed as a superposition of two stress distributions: one complying with the inner solution with static equivalents identical to those of the original stress distribution, while the other distribution has zero resultant force and moment. That second, self-equilibrated, load will induce end effects regarded as the outer solution for a given load. The displacement field describing these end effects for a semi-infinite plate is given by

$$\mathbf{u}(x,y) = \mathrm{Re}\left\{ \sum_n A_n \mathbf{U}_n(y) e^{i\xi_n x} \right\} \tag{2}$$

where $\xi_n$ are the (complex) eigenvalues of the Fadle-Papkovich equation, $\mathbf{U}_n(y)$ and $A_n$ are the eigenfunctions and their amplitudes, respectively. Here $\mathbf{U}_n(y)$ stands for a vector consisting of the $x$ and $y$ components of the displacement vector $\mathbf{u}$. Complex eigenvalues

$\xi_n$ make the solution (2) to decay in the axial direction $x$. The eigenvalue with the smallest imaginary part ($\xi_1$) dictates the extent of the outer solution – the largest distance from the end at which these decaying eigenfunction might have a non-negligible effect. Assuming the extent of the outer solution to be significantly smaller than the plate's length $l$, the complete expression for the axial strain in the vicinity of the clamped end can be written as

$$\varepsilon_x(x,y) = \frac{(1-\nu^2)(l-x)P}{EI} y + \mathrm{Re}\left\{ \sum_n A_n i\xi_n U_n^x(y) e^{i\xi_n x} \right\} \qquad (3)$$

where $U_n^x(y)$ is the axial component of the eigenfunction. It is understood of course that, in general, end effects will be induced at the loaded end $x = l$ as well. However, for future reference these end effects are omitted from (3) as they are not expected to practically influence the field in the vicinity of $x = 0$.

Several methods are available for calculating the amplitudes $A_n$ in a semi-infinite plate (e.g., [11], [12]). In these methods the resulting amplitudes should be such as to describe the detailed transversal distribution of the load (or displacement) at the edge $x = 0$. It is clear therefore that any alteration of load distribution over the width $2h$ will result in a change of the amplitudes. The eigenvalue with the smallest imaginary part dictates the upper bound on the smallest decay rate and has a value of $2.106/h$ for an elastic isotropic material. It follows that the eigenfunctions induce only insignificant contribution to the strain field beyond 1-2 beam widths. Any change in amplitudes $A_n$ will be significant only within that small range – the outer solution. Therefore, measurable changes of strains in the near field which are *not accompanied* by (practical) change of strains in the far field can be attributed to modification of end data leaving the static equivalents unaltered.

## *2.2. Dynamic End Effects*

Dynamic steady state (harmonic) displacement fields in a semi-infinite plate are commonly expressed by separation of variables

$$\mathbf{u}(x,y,t) = \mathrm{Re}\left\{ \sum_n A_n \mathbf{U}_n(y) e^{i(\xi_n x - \omega t)} \right\} \tag{4}$$

where $\xi_n$ are the wave numbers that solve the Rayleigh-Lamb frequency equation for any given frequency $\omega$, $\mathbf{U}_n(y)$ and $A_n$ are the wave mode vector and its amplitude, respectively. The spectral decomposition (4) can be considered as a dynamic generalization of the static solution (2). We use here the same notation $\xi_n$ for wave numbers as for eigenvalues in (2) as they bear the same meaning and coincide numerically upon reducing the Rayleigh-Lamb equation to the static case by taking frequency $\omega$ to zero. Methods for evaluating the amplitudes of the modes are similar to those used in the static case (e.g., [13], [14]), thus connecting the spatial distribution of the end data with the amplitudes of the evanescent waves. That connection facilitates the nature of end effects as a structural signature of end data.

Contrary to the static case, the full spectrum of wave numbers includes real valued roots ($\xi_n$) that correspond to propagating waves which convey energy into the far field. The evanescent waves associated with complex and purely imaginary wave numbers generate the end effects. This distinction between the two types of waves enables us to rewrite the solution (4) in the form

$$\mathbf{u}(x,y,t) = \mathrm{Re}\left\{ \sum_{n=1}^{N} A_n \mathbf{U}_n(y) e^{i\xi_n x} + \sum_{n=N+1}^{\infty} A_n \mathbf{U}_n(y) e^{i\xi_n x} \right\} e^{-i\omega t} \tag{5}$$

where the first summation is over the $N$ real valued wave numbers available at a given frequency $\omega$, while the second summation is over an infinite number of complex and

purely imaginary wave numbers. The propagating modes exhibit of course no attenuation (elastic response is assumed) in the axial direction of the plate, and therefore determine far field response. In a finite plate these modes develop eventually into vibration. The axial decay rate of the evanescent modes is highly sensitive to the excitation frequency, with very small values of imaginary parts of the wave numbers at some frequencies. Thus, no general conclusion relating to their maximal penetration depth can be reached in analogy with the static case [8]. Nevertheless, because the smallest imaginary part of the wave numbers is of the same order as in the static case, it can be expected that these attenuating waves will affect the strain field at least within the distance of 1-2 plate depths.

Solution (5) describes a steady state response to harmonic excitation with a given single frequency. Transient fields are taken as a superposition of these steady state solutions according to the Fourier theorem. Therefore, the observation that any change in the details of the end condition will influence amplitudes of the evanescent modes should be valid also for transient fields. Thus, as for the static case, if such changes in amplitudes of strain components, in the near field, can be detected by some sensitive device with no practical changes in strain readings appearing in the far field, for the same dynamic excitation, changes in end data can be inferred.

It should be mentioned that expressions (1)-(5) are valid under the assumption of plane strain conditions. The experiments, on the other hand, were performed with a beam, of finite width, for which neither plane strain nor plane stress can be justified. Representation of end effects, equivalent to those given in (2) and (5), for a three dimensional beam (neither plane stress nor plane strain) is given by Gregory [15] for quasi-static loading and by Wu and Plunkett [13], or by Vovk et al. [16], for dynamic response. The main added feature in the three dimensional analysis is that the

eigenfunctions (or wave modes) **U**($y$) become also dependent on the $z$ coordinate. That modification does not alter the fundamental property of end effects, discussed earlier, for plane problems as being structural markers reflecting details of end conditions.

## 3. Experiments

### *3.1. The Setup*

In the design of the experiments the immediate aim was to examine how different clamping conditions will influence the strain field within a plate subjected to transverse load. Particularly, we wished to demonstrate the sensitivity of the surface strain in the vicinity of the clamped end of the beam to different ways in which clamping is realized. No attempts were made to make quantitative assessments or to develop predictive tools, as those are expected to be tailored for each specific application. The particular function required of the system is to record surface strain response in the near and far fields of a beam subjected to identical static loads and dynamic excitations for various clamping conditions.

A cantilever beam made of Aluminum alloy 6061-T3 ($E$ = 69.3 GPa , $\nu$ = 0.33), with dimensions detailed in Fig. 1, is clamped with the aid of 6 screws, arranged in two rows, to another vertical beam. The reference state of all screws "tight-in" is considered as a *baseline* clamping condition. Controlled variations of clamping conditions were achieved by unscrewing, either partially or completely, one or more screws.

Static and dynamic loads were applied at the free end of the beam. Five strain gauges with a gauge length of 2 mm were attached to the upper surface of the beam along its centerline at distances of 5.7, 12.5, 25.4, 100, 200 mm from the clamped end (corresponding to non-dimensional distances $x/2h$ of 0.2244, 0.49, 1, 4, 7.9) and designated here as *stations* 1 to 5, respectively. The strain gauges were sampled at the

rate of 100 kHz/16-bit with a gain of 200. For static loads the signal was averaged 1000 times to improve signal to noise ratio.

### *3.2. Quasi-Static Experiments*

The static load was chosen to be a transverse dead load applied at the free end ($x = l$) to induce bending of the beam. An appropriate weight was hinged on a screw located at the centerline of the beam at the free end. The experiments consisted of repeating the static loading for various (controlled) clamping conditions. To simulate practical situations of damage two cases of missing screw(s) were tested: releasing the screws prior to loading and changing their tightening while the beam is under constant load. The first set of experiments examined the on/off condition of the screws while in the second set the ability to identify different levels of tightness was addressed. For that purpose a torque-meter was used in tightening the screws. The strains expected to develop within the beam are as predicted by (3) with some deviation attributed to the three dimensional nature of the field within the beam.

It should be noted that the strains within the beam do not vanish even if no load is applied at its end at $x = l$ (and with gravity being neglected). This is due to the self-equilibrated load applied at the built-in end by the screws, leaving (3) only with the second term of summation over the eigenfunctions. For that reason the reading of the gauges in the dynamic experiments had to be readjusted to zero following any change in the clamping conditions.

### *3.3. Dynamic Experiments*

As a simple way of providing dynamic excitation an impact by an aluminum rod (length 158 mm and diameter 12.5 mm) at the free end of the beam was used. The impacting rod was dropped from the high of 275±5 mm above the beam generating a bending pulse

with an approximate duration of 50 μs. Repeated impacts were avoided by catching the rod upon its bouncing off the beam. Since repeatability of the excitation is critical in interpretation of the experiments, an attempt has been made to generate as identical an input as possible. Although a simple device for marking the drop position was used, this handy method of dynamic excitation was not expected to deliver a highly repeatable input, and probably inferior to the widely used pulse generators (i.e., PZT). Nevertheless, the simple procedure employed turned out to be satisfactory for the purposes of this research.

The beam with various clamping conditions was excited by dropping the aluminum rod, approximately from the same height, to hit the center line of the free edge of the beam. Each drop was considered as a single experiment. This excitation generated bending waves which propagated towards the clamped end and back, eventually inducing vibration of the beam. Due to the transient nature of the response, the signals recorded are the superposition of eigenfields expressed by the summation (5), for as many frequencies as contained in the excitation itself. It should be noted that evanescent waves are expected to be induced also at the free end of the beam $x = l$. It is assumed however that these evanescent waves have no influence on all five strain gauge readings, which are located closer to the clamped end. It is worth noting that though the strain gauges in the near field were expected to record superposition of incoming and reflecting signals, it does not impair the purpose of the research, as no interpretation of that superposition is attempted here.

Strain gauges readings were zeroed prior to each experiment, to cancel out the shift of the output, induced by quasi-static change of strains due to removal of screws. Repeatability of the system was checked at various stages of the experiment and used for interpretation of the results.

# 4. Results

## *4.1. Static Loading*

The beam was loaded statically by a dead load of 110 N at its free end. Then, the screws were loosened and retightened back, one at a time. The strain history of that sequence was traced in Fig. 2. The figure shows clearly that, as expected, the three strain gauges located within the near field (stations 1, 2, 3) responded significantly to the removal of each screw. Release of the screws in row B, located at larger distances from the strain gauges (screws B1 and B2), induced smaller effects than those closer to the strain gauges (screws A1 and A2). This difference is probably due to compression below the neutral plane, leaving screws in row B only with secondary function as compared to the function of the screws in row A. For future reference it is noted that the effect of missing screws B1 and B2 is practically identical. As expected, the two strain gauges at stations 4 and 5, located in the far field, did not record any change of strain due to changes in the clamping condition. Some hysteresis upon retightening the screws can be observed, probably due to uncontrolled screwing moment at this stage of the experiments.

Strain recordings for the beam when loaded with 20 N and 110 N for three clamping conditions are shown in Figs 3 and 4, respectively. Theory of elasticity solutions, for the bending problem, in plane stress and plane strain, are given by

$$\varepsilon_x(x)\big|_{y=h} = \frac{(l-x)P}{EI}h \qquad \text{plane stress} \tag{6}$$

$$\varepsilon_x(x)\big|_{y=h} = \left(1-\nu^2\right)\frac{(l-x)P}{EI}h \qquad \text{plane strain} \tag{7}$$

and displayed in Figs. 3 and 4, for the two loads. The connecting lines between the measurement points are for the sake of visualization. As expected, the recordings of strain gauges in the far field (stations 4 and 5) lie within the limits of the prediction given

by the theory of elasticity (6) and (7). Recordings of the gauges located in the near field (stations 1-3) deviate significantly from both these lines and from the straight line that could be extrapolated based on measurements at stations 4 and 5. That deviation indicates the dominance of the decaying modes, of the type given by (2), over the inner solution (6)-(7), in the surface strain within the immediate vicinity to the joint. A discussion of Figs. 3-4, in relation to Saint-Venant's principle, will be given later.

Fig. 5 shows recordings of all 5 stations for a sequence of different torque levels of screw A3 while the beam is loaded with 110 N. Prior to application of the load the screws were tightened with a torque of 250 N·cm and the strain gauge readings were zeroed. Then the beam was loaded, screw A3 was removed completely followed by its retightening with intermediate pauses at torque levels of 100, 175 and back to 250 N·cm.

It may be concluded from these results that it is possible to identify changes in the clamping details (joint condition). Such detection of even relatively small changes in the joints is based on the measurements of strain within the range of dominant end effects. Measurements taken from regions located far from the joint do not provide a similar indication.

### *4.2. Dynamic loading*

A typical long time strain history for the dynamic experiment is shown in Fig. 6 for three different clamping conditions. The first vibration mode is clearly visible with a natural frequency of 33 Hz – lower than the calculated one (50 Hz) due to flexibility of the supporting beam. A pattern of almost pure vibration is observed after three time periods (≈90 ms). It takes approximately 0.2 ms for a shear wave and 0.1 ms for a longitudinal wave to travel across the length of the beam. Therefore, the recording at any station within the time interval of 30 ms is a superposition of several waves propagating in

opposite directions, making a direct connection between the recordings and the displacement field (5) impractical. Yet, some conclusions can be inferred since the amplitude of the recorded signal is a superposition of all available modes at all excited frequencies. This will be done by focusing mainly on the amplitude of the response within the first 10-20 ms of the transient response.

The dynamic response at stations 2 and 5 for baseline and clamping without screws A2 or A1 are shown in Fig. 7. At station 5 no difference in response for these three clamping conditions can be noticed, while at station 2 deviation from the baseline is significant, as can be judged from repeated experiments. Repeatability of the recordings at station 2 for baseline (three identical experiments) and for missing screw A1 (two experiments) are shown in Fig. 8. The results for different clamping conditions at station 5, as shown in Fig. 7b, fall within the scatter of experimental repeatability and therefore different clamping conditions cannot be inferred from measurements at station 5.

It is instructive to compare the recordings of Fig. 7a with those of Fig. 7b in view of the partition into two types of waves, as given by (5). Assuming that station 5 lies in the far field, it is not influenced by end effects and consists only of propagating waves contained in the first summation of (5). Previous results for static loading, as well as numerical values of complex wave numbers [8] (with the exception of small frequency range adjacent to cut off frequencies) support this assumption. Thus, identical strain responses recorded at station 5 (Fig. 7b) for different clamping conditions can be attributed to generation of the same $N$ propagating wave modes with identical amplitudes for all three different clamping conditions. It may be argued therefore that dynamic excitation applied at the end is practically identical for all experiments shown in Fig. 7.

The recordings at station 2 (Fig. 7a) are a superposition of all available modes and frequencies. Here, unlike readings at station 5, the strain amplitude is a superposition of propagating and evanescent waves. Thus, the partition of (5), together with the

conclusion that the excitation is practically identical (identical propagating waves), leads to conclusion that the different recordings at station 2 are due to different generation of evanescent waves. This, as expected, makes the connection between the joint condition and the evanescent waves in analogy with the static experiments.

In Fig. 9 the recording for baseline clamping at station 2 is compared with the recordings for clamping when one of the lower screws (B1 or B2) is missing. Only minor changes in response due to the absence of screws B1 or B2 is noticeable in agreement with the static results shown in Fig. 2. Recording of these two cases for stations 1 and 3 are given in Figs. 10 and 11, respectively. It can be observed that the strains at station 1 are sensitive enough to enable identification of missing screws B1 and B2, though recordings for the two are indistinguishable. Similar effects induced by missing screws B1 and B2 could be expected from the static results in Fig. 2. Taking out screws B1 or B2 does not alter significantly enough the reading at station 3, neither in the static case (Fig. 2) nor in the dynamic case (Fig 11) (though in the static case a small change is noticeable).

Fig. 10 displays the zoom-in of the first 10 ms of the response shown in Fig. 6. We find that for both short-time and long-time response, it is possible to distinguish between the baseline condition and the state of missing screws. It is apparent from Fig. 6 that the frequency of this vibration mode is not altered by removal of one screw from the lower row B. This suggests that the amplitude of the strain in the near field is more sensitive to small changes in the joint, as compared with the natural frequency. It appears that the amplitude of the strain in the near field is preferable to the natural frequency, as a marker for the joint condition. Moreover, either steady state or transient response of the beam can be used for health monitoring, if the diagnostic parameter is the near field amplitude.

Recordings at station 2 for two cases, when two or three screws are missing, are

compared with the baseline state in Fig. 12. The change in pattern is considerable, accompanied by profound change in the natural frequency of vibration. To ensure repeatability, after the recordings of Fig. 12, all screws were put in place and the original signal (Fig. 8a) was recovered. The shift in the natural frequency, induced by relatively large changes in joint condition, leads to vibration-based diagnostic methods, which is fully supported by this study. An equivalent reliance on natural frequency as a marker for minor changes in joint conditions, as revealed in Figs. 6-11, does not appear to be feasible. That observation will be supported by an FFT analysis in the next section.

## 5. Discussion

The static phase of the experiments was designed primarily in order to assess the sensitivity of the system subsequently employed in dynamic experiments. It was expected, from the similarity of (3) and (5), that joint damage detectable by static experiments will be exposed with dynamic loading as well. The static measurements shown in Figs. 2-5 display considerable sensitivity of the near field to complete absence of a single screw at various locations, and even to partially loosened screws. Moreover, loss of screws located in the compressive region (row B), where the screws have a smaller contribution to the joint's rigidity, is also detectable by measurement of surface strain in the near field.

Inter alia, Figs. 3-4 provide an interesting demonstration of regions of validity of Saint-Venant's principle. Existing experimental demonstrations of the Saint-Venant region are based mainly on the photoelastic method [17]. Deviations of measured surface strain from the linear predictions (6)-(7) illustrates the extent of the Saint-Venan't region which is definitely larger than one height of the beam ($2h$).

Interpretation of the dynamic experiments relies here on both the *pattern* and

*amplitude* of the signal, in time domain of near field strain. Fig. 12 shows an extreme response that occurs when the clamping condition is substantially altered. It can be easily detected by strain gauges located in the near field, when the structure is dynamically excited. However, such a large change in clamping condition is also recorded by the remote stations. Thus, there is no gain in locating strain gauges in the near field when large changes in the joints' rigidity are to be monitored.

A more subtle result is sought when only small changes in joint strength take place, such as the loss of only one screw, that might not be detectable by gauges located in the far field. Figs. 7a and 10 show that removal of a single screw, either in the tensile or in the compressive regions of the built-in edge, alter significantly the pattern of surface strain response in the near field but not in the far field. In the analogy with the static case, the dynamic near field differs from the far field by active decaying modes which reflect details of the end data. That connection between end conditions and evanescent waves justifies the use of end effects as a *joint signature* which serves as a *marker* for monitoring the joint condition. It is beyond the scope of the present paper to discuss types of damage that should be considered as major (affecting the natural frequency), as opposed to minor damage detectable only by the near field signature. It is conceivable however that this clarification depends on specific applications.

In Figs. 7-12 we have focused on transient response of the beam which can be achieved in practice by a pulsating wave generator. Comparing Fig. 6, which is typical to a vibrating structure, with Fig. 10 we find that screw removal can be detected either by inspection of the transient response or through the steady state vibration. Hence, when the structure vibrates during its operation it should be possible to identify changes in joints condition without resort to auxiliary dynamic excitation. On the other hand, if the structure does not vibrate, as is often the case with space structures, small devices

generating propagating Lamb waves directed toward the joint will serve the same diagnostic purpose. That, of course, is in cases when static measurements are not a feasible possibility.

An interesting difference between static and dynamic experiments is the higher sensitivity of static tests that enabled detection of low levels of tightness of screws. It is expected that with some minor improvements of the equipment (e.g. smaller strain gauges and more repeatable dynamic excitation) it will be possible to detect partially loose screws in dynamic tests as well.

It is of interest to compare the above analysis of near field response in the time domain with vibration-based measurements. To this end an FFT analysis was performed on the data of the experiments shown in Fig. 7. The corresponding FFT plot of the recording at station 2, the time domain of which is shown in Fig. 7a, is traced in Fig. 13 for baseline clamping and for clamping with missing A2 screw. Two dominant frequencies of 33 Hz and 50 Hz (and its higher harmonics) are clearly seen. The peak frequency of 244 Hz appears to be that of the second vibration mode of a cantilever beam clamped to a less than perfectly-rigid support (theoretical frequency of the second mode is approximately 310 Hz for a beam in plane stress). The main difference between the two plots of Fig. 13 is a higher amplitude of the peak frequency at 67.1 Hz upon removal of screw A2. That can be correlated with the major signal change in time-domain shown in Fig. 7a. Marginal shift of the frequency from 244 Hz to 241 Hz can also be noticed in Fig. 13.

A similar comparison of FFT plots of the recordings at station 5, for baseline clamping and for two cases of missing screws A1 and A2, shown in Fig. 7b, reveals almost identical curves. The recording at station 5 can be considered as data from a

representative location commonly used in vibration-based methods. Only few marginal variations are detectable (and therefore not shown here): shift of the 244 Hz peak frequency to 241 Hz and a slightly larger amplitude of a peak at 67 Hz. This agrees with the known observation that the lowest natural vibration frequencies exhibit only low sensitivity to end conditions.

## 6. Concluding Remarks

The possibility to identifying changes in end data details through measurements of surface strain, in the close vicinity to the joint, has been examined. Strains were measured by standard gauges while the joint condition was controlled by loosening and retightening of screws. It was demonstrated that it is feasible to detect loss of one screw out of six and even to detect intermediate levels of loosening of the screws. Only marginal changes in natural frequencies were observed in far field measurements. It appears that it is more effective to establish health monitoring, either in the time or in frequency domains, on measurements taken from the field near to the joint. Commercially available, simple wave generators are believed to provide similar results, with even better repeatability, and with improved overall sensitivity of the method.

The nature of Lamb waves and of evanescent modes restricts application of the suggested method to joints connecting plate-like (or beam-like) structural members. The end effect sensitivity demonstrated here can be used as a joint signature for identification of incipient damage or deterioration and for a variety of joint types: bolted, welded, bonded, or riveted. High sensitivity is what makes the suggested method attractive and applicable in detecting early stages of damage.

The health monitoring method suggested here is of local nature, so there is probably a limit on the number of joints that can be monitored. Nevertheless, the sensitivity of end

effects, found here in reflecting joint integrity, renders this method a good candidate to be used as a supplementary diagnostic method for critical joints. The procedure can be integrated into a global structural health monitoring system envisioned for future structures (e.g., [18]).

## Acknowledgments

This work has been supported by the Asher Space Research Fund at the Technion. One of the authors (B.K.) wishes to express his thanks to the kind hospitality of the Faculty of Aerospace Engineering, Technion, Haifa.

## References

[1] O.S. Salawu, Detection of structural damage through changes in frequency: a review. *Engineering Structures* 19 (1997) 718-723.

[2] E.P. Carden, P. Fanning, Vibration based condition monitoring: A review. *Structural Health Monitoring* 3 (2004) 355-377.

[3] S.W. Dobeling, C.R. Farrar, M.B. Prime, W. Daniel Shevitz, Damage identification and health monitoring of structural and mechanical systems from changes in their vibration characteristics: a literature review. *LANL report* LA-13070-MS (1996).

[4] C.R. Farrar, S.W. Doebling, D.A. Nix, Vibration-based structural damage identification, *Phil Trans R Soc London A: Mathematical, Physical and Engineering Sciences* 359 (2001) 131-149

[5] H. Sohn, C.R. Farrar, F.M. Hemez, D.D. Shunk, D.W. Stinemates, B.R. Nadler A review of structural health monitoring literature. 1996-2001. *LANL report* LA-13976-MS (2003).

[6] Z. Su, L. Ye, Y. Lu, Guided Lamb waves for identification of damage in composite structures: A review. *Journal of Sound and Vibration* 295 (2006) 753-780.

[7] P. Pandurangan, G.D. Buckner, Vibration analysis for damage detection in metal-to-metal adhesive joints. *Experimental Mechanics* 46 (2006) 601-607.

[8] B. Karp, D. Durban, Evanescent and Propagating Waves in Prestretched Hyperelastic Plates. *International Journal of Solids and Structures* 42 (2005) 1613-1647.

[9] B. Karp, Dynamic version of Saint-Venat's principle - Historical account and recent results. *Nonlinear Analysis* 65 (2005) e931-e942.

[10] R.D. Gregory, F.Y.M. Wan, Decaying states of plane strain in a semi-infinite strip and boundary conditions for plate theory. *Journal of Elasticity* 14 (1984) 27-64.

[11] P.J. Torvik, The elastic strip with prescribed end displacement. *Journal of Applied Mechanics, Transactions of ASME* 38 (1971) 929-936.

[12] M.E. Ducan Fama, Radial eigenfunctions for the elastic circular cylinder. *Quarterly Journal for Mechanics and Applied Mathematics* 25 (1972) 479-495.

[13] C.-H. Wu, R. Plunkett, On the solutions of plates, strips, rods, and cylinders subjected to arbitrary dynamic edge load. *SIAM Journal Applied Mathematics* 15 (1967) 107-119.

[14] W.M. Karunasena, A.H. Shah, S.K. Datta, Reflection of plane strain waves at the free edge of a laminated composite plate. *International Journal of Solids and Structures* 27 (1991) 949-964.

[15] R.D. Gregory, The general form of the three-dimensional elastic field inside an isotropic plate with free faces. *Journal of Elasticity* 28 (1992) 1-28.

[16] A.E. Vovk, V.V. Gudkov, T.V. Levchenkova, V.V. Tyutekin, Normal modes of a solid rectangular waveguide. *Soviet Physics Acoustics* 26 (1980) 194-198.

[17] M.M. Frocht, *Photoelasticity*. Vol. II, John Wiley & Sons, Inc., New York (1948).

[18] E.R. Generazio, *Overview of the National Aeronautics and Space Administration's Nondestructive Evaluation (NDE) Program*, 38 Quality Assurance and Reliability, NASA, June 1999 (1999).

**Figure(s)**

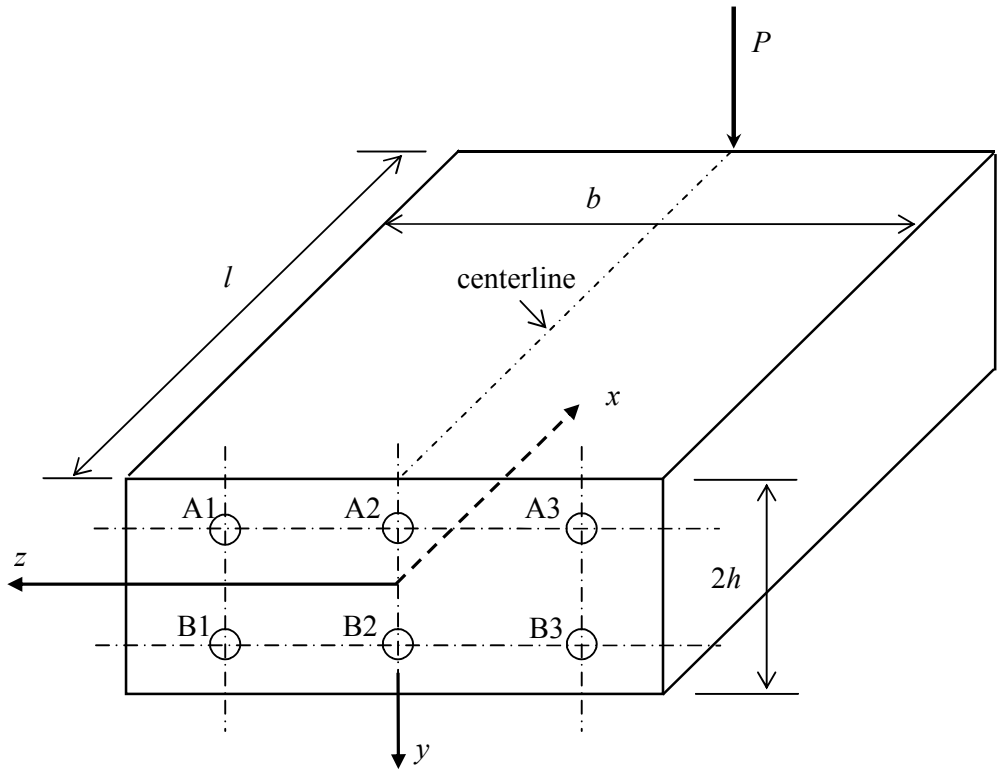


**Fig. 1** – Schematic view of the elastic beam and the clamped end showing the coordinate system, the numbering of the six screws (A1 – B3) at the clamped end, the load location at the free end, and centerline along which strain gauges were aligned. At the free end $x = l$ either quasi-static or dynamic bending load $P$ is applied. In the experiments a beam with dimensions of $l$=665 mm, $2h$=25.4 mm, $b$=60 mm was used.

**Figure(s)**

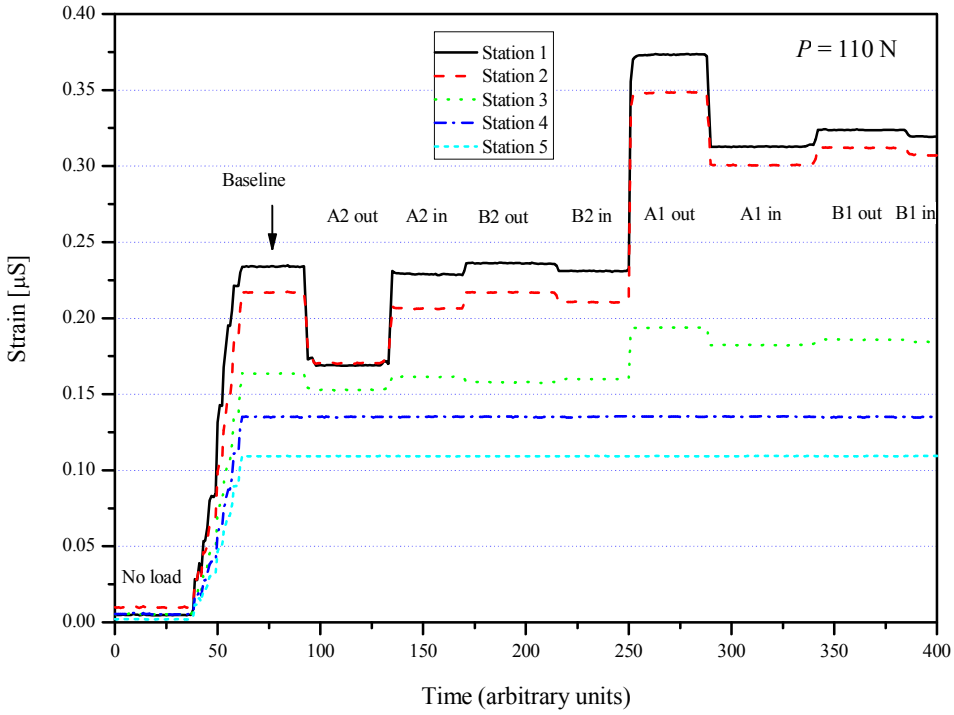


**Fig. 2** – Strain history at five stations for a sequence of removal and retightening of screws with an end load of 110 N.

**Figure(s)**

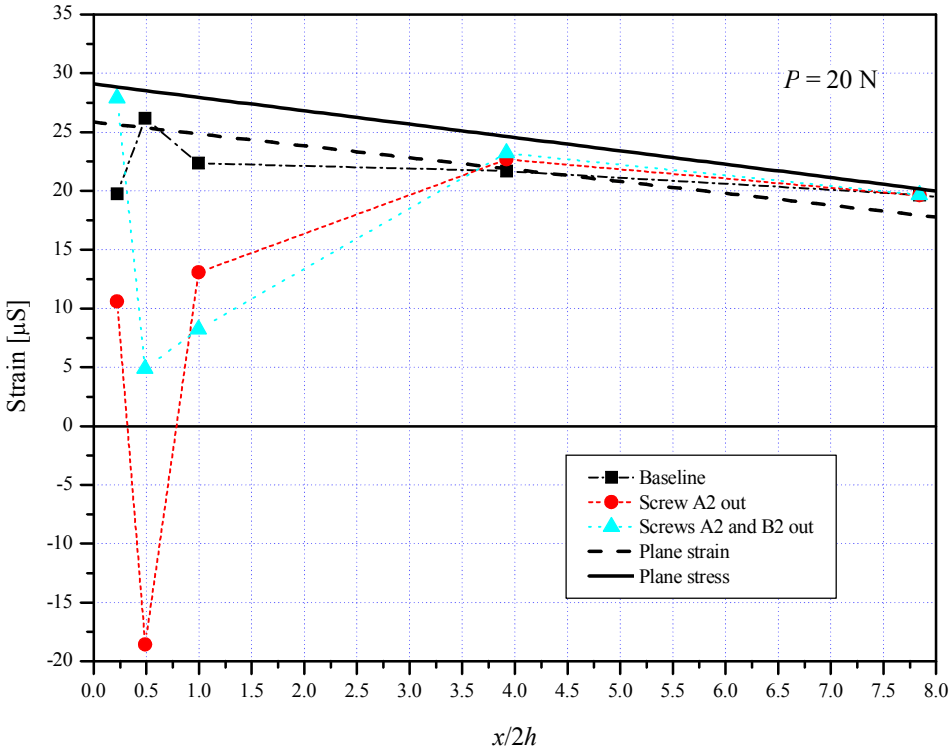


**Fig. 3** – Strain at five stations for three clamping conditions (baseline, missing screw A2, missing screws A2 and B2) with an end load of 20 N.

**Figure(s)**

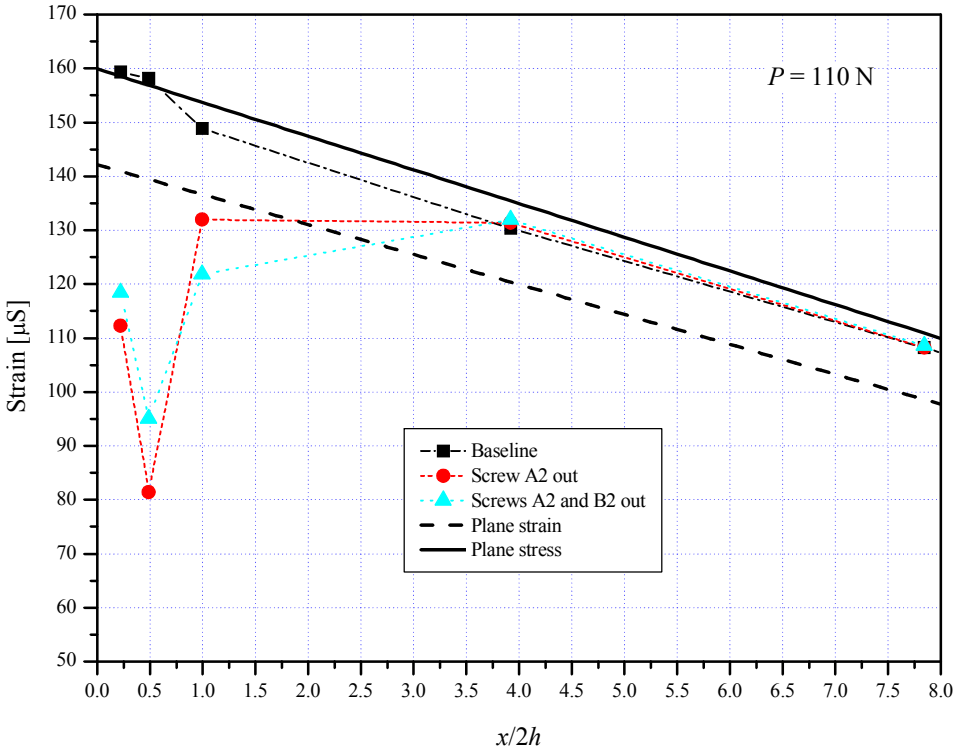


**Fig. 4** – Strain at five stations for three clamping conditions (baseline, missing screw A2, missing screws A2 and B2) with an end load of 110 N.

**Figure(s)**

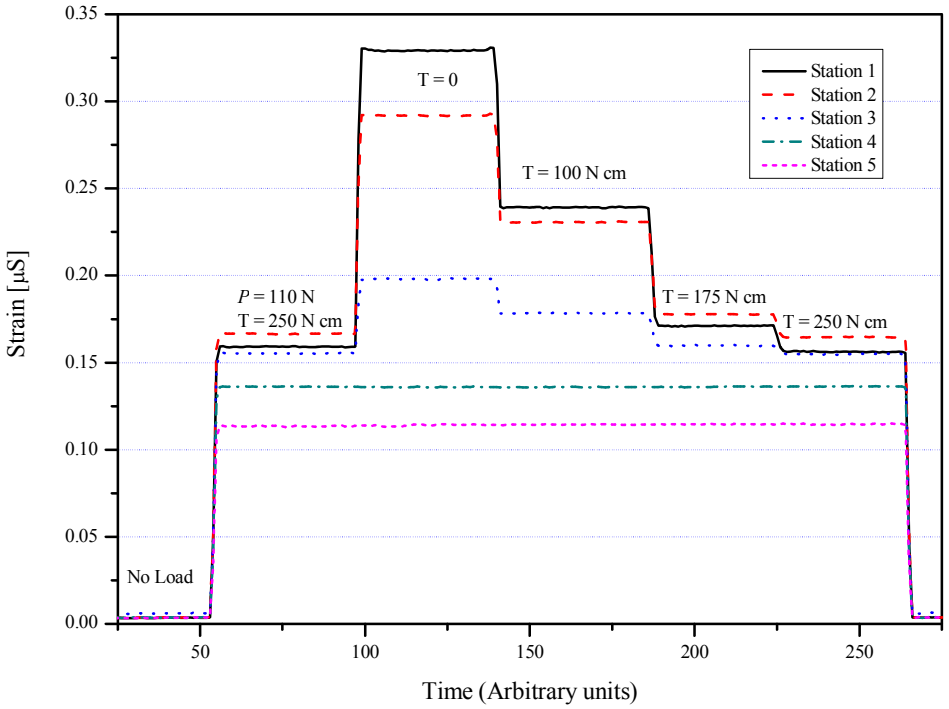


**Fig. 5** – Strain at all five stations for a sequence of torque levels T [N cm] of screw A3. The beam is loaded by a dead load of 110 N.

**Figure(s)**

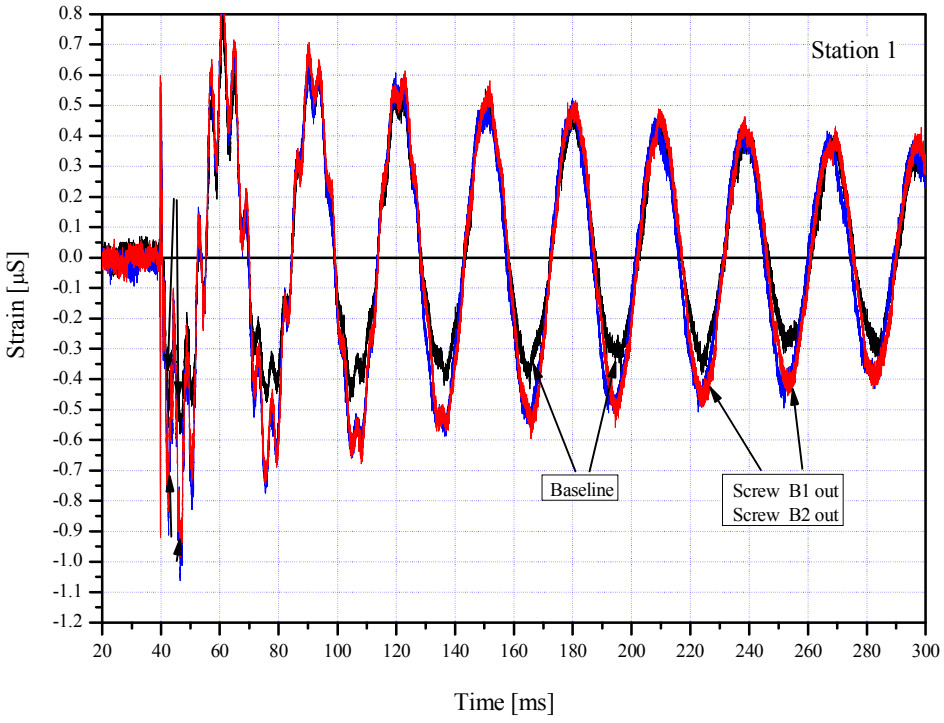


**Fig. 6** – Strain at station 1 for three identical experiments with different degrees of clamping. Recordings for screws B1 out, and B2 out, are almost identical.

**Figure(s)**

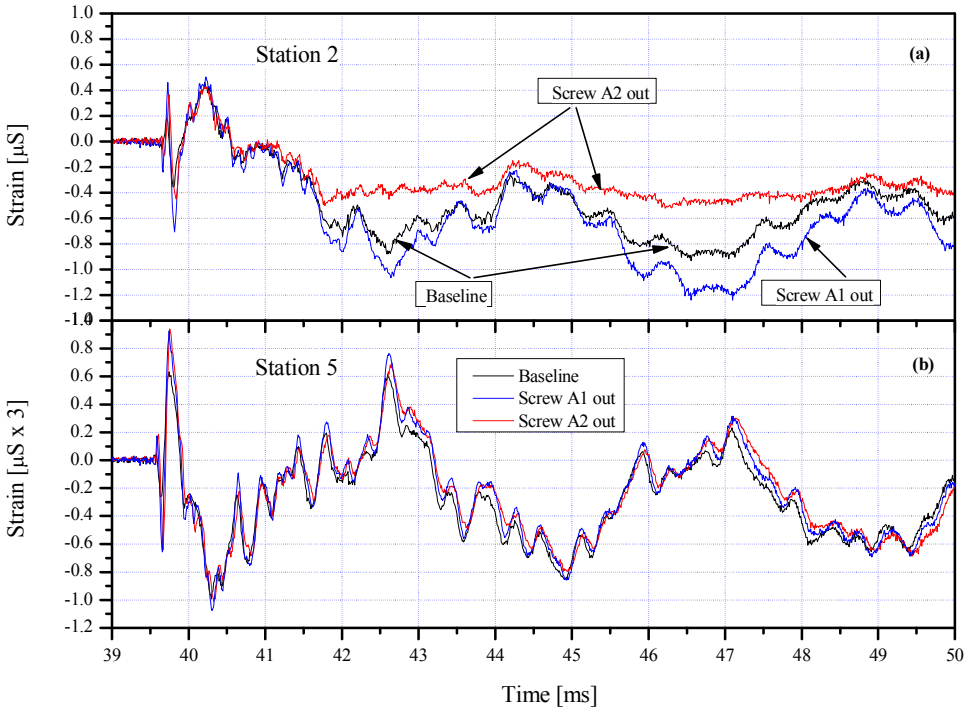


**Fig. 7** – Strain at stations 2 and 5 for baseline clamping and for clamping without screws A2 or A1: (a) station 2; (b) station 5.

**Figure(s)**

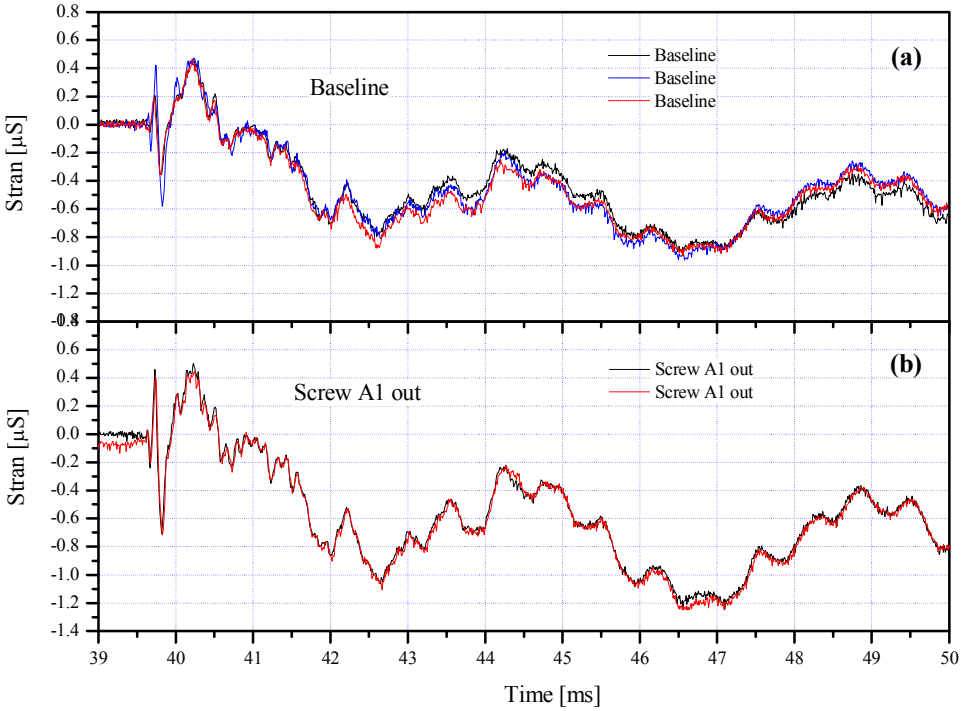


**Fig. 8** – Strain at station 2 for two sets of repeatability verifications: (a) three identical experiments with a baseline clamping; (b) two identical experiments with missing screw A1.

**Figure(s)**

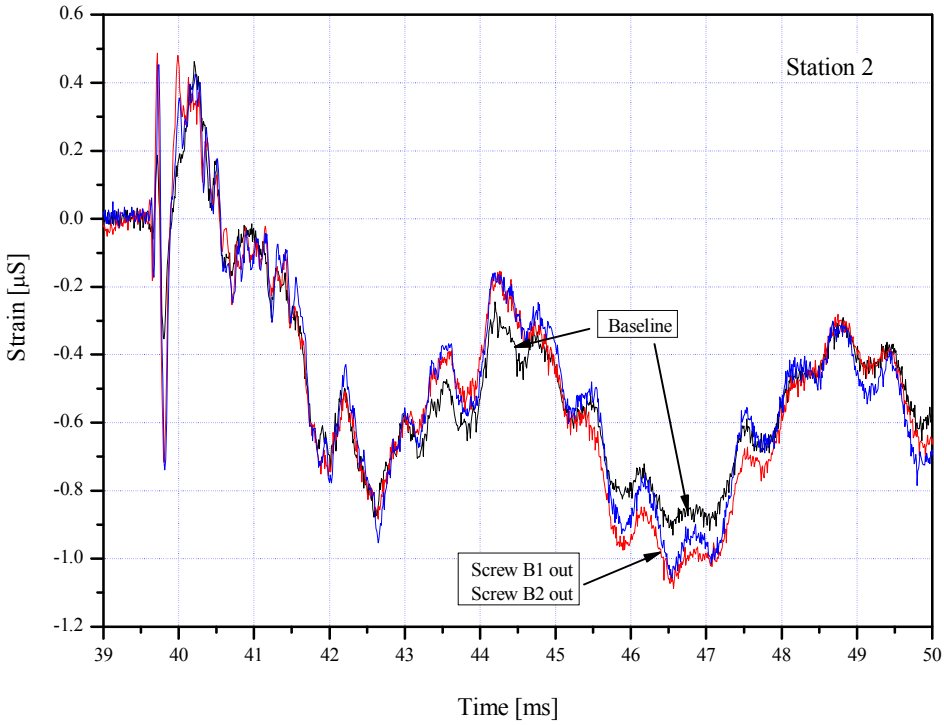


**Fig. 9** – Strain at station 2 for baseline clamping and for clamping without screws B1 or B2. Recordings for screws B1 out, and B2 out, are almost identical.

**Figure(s)**

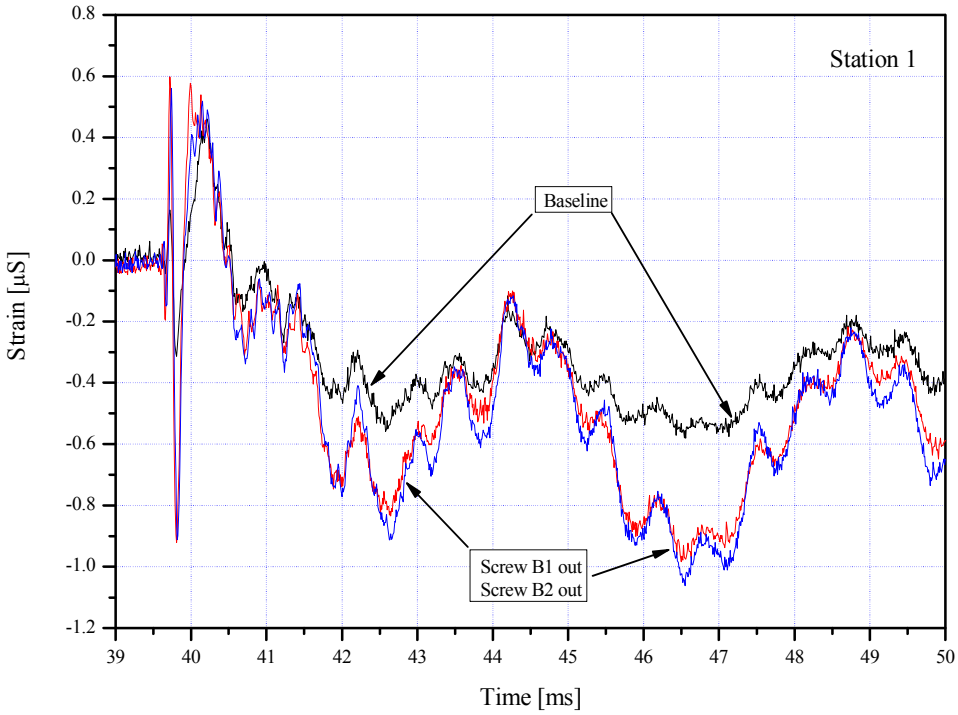


**Fig. 10** – Strain at station 1 for baseline clamping and for clamping without screws B1 or B2. Recordings for screws B1 out, and B2 out, are almost identical.

**Figure(s)**

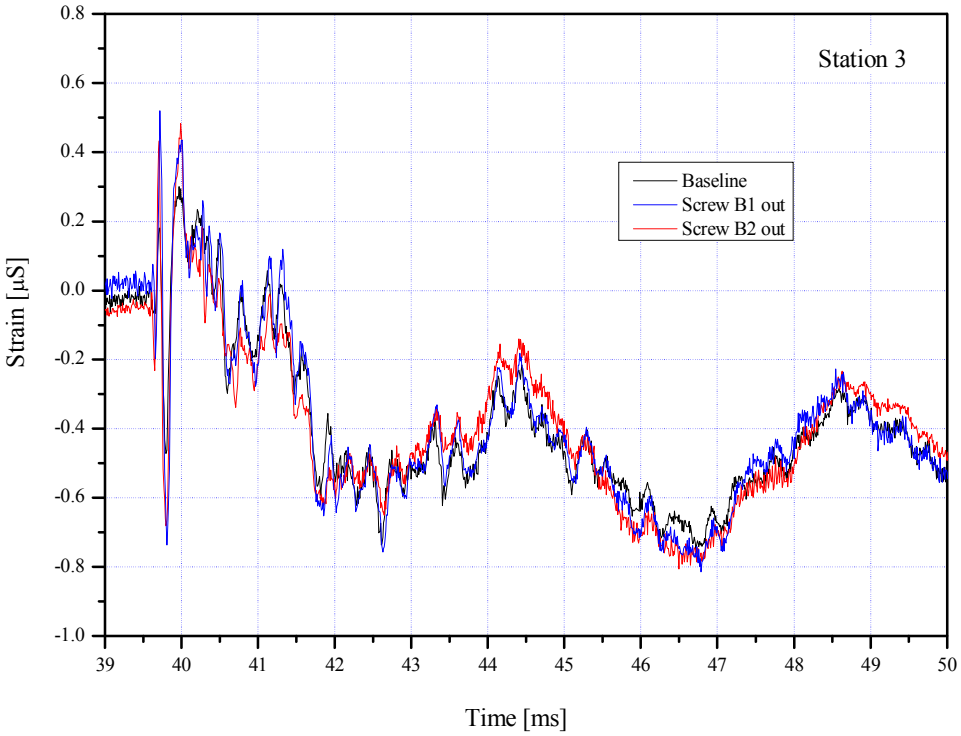


**Fig. 11** – Strain at station 3 for baseline clamping and for clamping without screws B1 or B2. The three recordings are indistinguishable.

**Figure(s)**

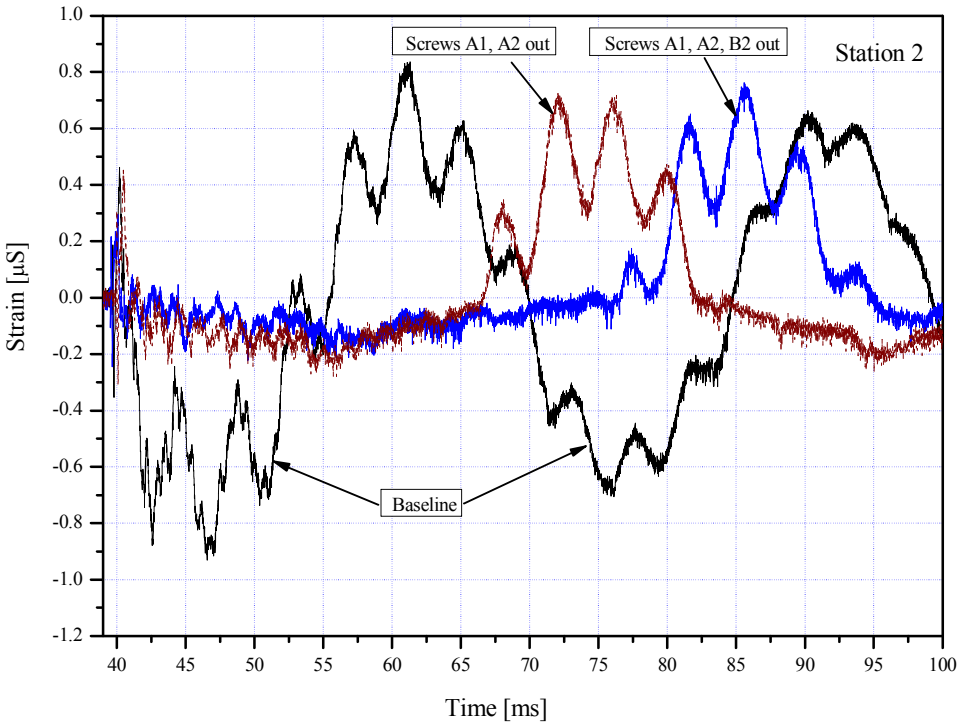


**Fig. 12** – Strain at station 2 for three clamping conditions with more than one screw missing.

**Figure(s)**

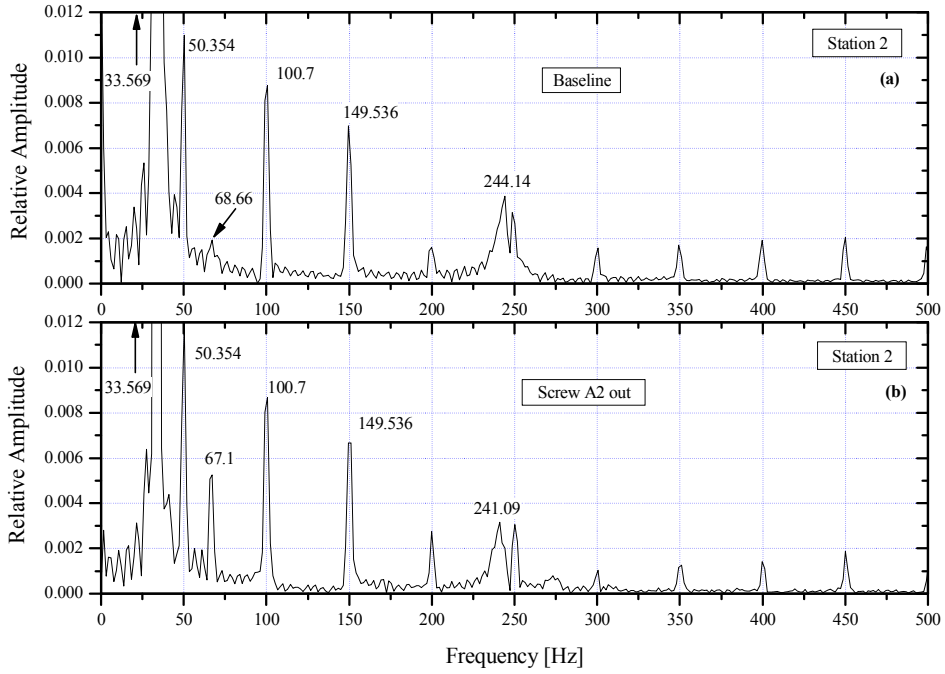


**Fig. 13** – FFT of the recording at station 2: (a) for baseline clamping; (b) for clamping with missing A2 screw.